ACS OMEGA

Article

Cite This: ACS Omega 2019, 4, 20197−20204

http://pubs.acs.org/journal/acsodf

Stereolithography 3D Printing of Lignin-Reinforced Composites with Enhanced Mechanical Properties

Shuyang Zhang,[†] Mi Li,[†,‡] Naijia Hao,[†] and Arthur J. Ragauskas*[,†,‡,§]

[†]Department of Chemical and Biomolecular Engineering, The University of Tennessee, Knoxville, Tennessee 37996, United States

[‡]Joint Institute for Biological Sciences, Biosciences Division, Oak Ridge National Laboratory, Oak Ridge, Tennessee 37831, United States

[§]Department of Forestry, Wildlife and Fisheries, Center for Renewable Carbon, The University of Tennessee Institution of Agriculture, Knoxville, Tennessee 37996, United States

Supporting Information

ABSTRACT: Due to the availability, biodegradability, and biological effects, lignin has emerged as an interesting alternative to petroleum-based compounds for developing sustainable chemicals, materials, and composites. In this study, lignin at various concentrations was incorporated into methacrylate resin via solution blending to fabricate lignin-reinforced composites using stereolithography apparatus three-dimensional printing. Softwood kraft lignin in the amounts of 0.2, 0.4, 0.5, 0.8, and 1.0 wt % in the methacrylate resin was used as a printing ink, and the gel contents and relative contents of the residual resin in the printed samples with various lignin concentrations were measured. The effects of the lignin on the ultimate mechanical properties of the non-postcured and postcured printed composites were determined. The tensile testing results revealed that the incorporation of lignin in the composite increased the tensile strength by 46−64% and Young's modulus by 13−37% for the postcured printed composites compared with that of the control sample (no lignin added). Employing a 0.4 wt % softwood kraft lignin, the tensile strength of the postcured printed composite reached the highest value of 49.0 MPa, which was a 60% increase in comparison to that of the control sample with 30.7 MPa. Scanning electron microscopy images of the fracture samples illustrated that the lignin-incorporated composites exhibited a rougher fracture surface that can presumably dissipate the stress, which could be a contributing factor for the mechanical enhancement.

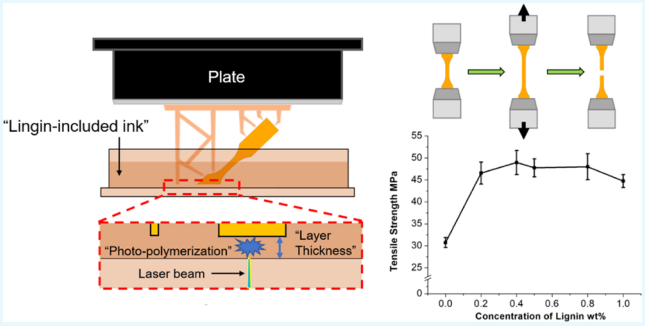

1. INTRODUCTION

Three-dimensional (3D) printing is a computer-aided additive manufacturing method that has gained growing attention due to its capability to fabricate high-shape-complexity products without molds.[1] Several techniques, such as fused deposition modeling (FDM), direct ink writing, powder bed fusion, binder jetting, vat photopolymerization, sheet lamination, and stereolithography, have been applied in the 3D printing process. Among these techniques, the stereolithography apparatus (SLA) uses UV light to solidify and cure a liquid ink through photopolymerization that allows for superior accuracy control and high resolution (up to 10 μm/layer) during the layer-by-layer printing process.[2] However, the requirement of photoreactive resin in stereolithography narrows the selection of the starting material[2] and, in turn, limits the applications of the resultant products. To overcome this shortcoming and obtain SLA products with various functions, researchers have developed various types of modified photoreactive resins.[3−8] One of the methods is blending fillers with resins. For example, carbon materials, such as graphene oxide and carbon nanotubes, renowned for their high-performance mechanical properties, were added as enhanced fillers in the resin system to improve the mechanical performance of the printed materials.[4,9,10] Apart from carbon materials, other inorganic particles (nanoclay, aluminum oxide nanowires, sepiolite nanofibers, TiO_2, and SiO_2) have also been incorporated into the stereolithography process.[11−13] These reports suggest that the incorporation of fillers in photoreactive resins is a promising means to improve the mechanical properties of the SLA-printed products.

Of the many additives available, lignin shows significant research interest, particularly in the advent of bioeconomy.[14] With the addition of lignin as a filler, a variety of studies have shown that the resulting polymeric composites exhibit improved physical properties including antiaging,[15] flame retardant,[16] and UV absorption.[17] 3D-printed lignin-based materials have been investigated for the application as drug-delivery materials[18,19] and bio-based plastics and composites for scaffold in the medical engineering area.[19] From the perspective of improving the mechanical properties of

Received: August 2, 2019
Accepted: November 7, 2019
Published: November 20, 2019

DOI: 10.1021/acsomega.9b02455
ACS Omega 2019, 4, 20197−20204

composites, lignin can be employed as a stiff filler,[10,13] in much the same manner as it performs in vascular plants contributing to cell wall rigidity and durability. Therefore, several researchers had applied lignin in the field of 3D printing for biomaterials and composites, and studied on the reinforcement of lignin on the printed materials. Using an FDM 3D printing technique, Nguyen et al.[20] have shown that the incorporation of hardwood lignin (40 wt %) into nylon 12 increased Young's modulus of printed samples from ∼1.77 to ∼3.01 GPa and maintained the tensile strength at ∼55 MPa. The authors attributed the enhancement to the rigid phenolic units in lignin. This type of reinforcement in modulus may also be ascribed to the potential hydrogen bonds between lignin and nylon according to the report by Sallem-Idrissi et al.[21] Gkartzou et al.[22] reported the reinforcement of pine kraft lignin in FDM-printed sample of polylactide/lignin composite at various lignin concentrations. The Young's modulus of composites increased from ∼2.31 GPa (0 wt % lignin) to ∼2.33 GPa (5 wt % lignin), 2.41 GPa (10 wt % lignin), and ∼2.39 GPa (15 wt % lignin), while the tensile strength decreased with more lignin being added. Mimini et al.[23] compared the influence of kraft lignin, organosolv lignin, and lignosulfonate on the flexural and impact strengths of FDM-printed composite with PLA. The results showed a slight reduction on both flexural and impact strengths with blending 5, 10, and 15 wt % of the three species of additive. In terms of stereolithography 3D printing, Feng et al. printed composites with methacrylate/lignin-coated cellulose resin. They found that 0.5 wt % or less lignin-coated cellulose nanocrystals in the printed composite slightly improved the tensile strength and modulus of the postcured samples. However, the tensile performance dropped down when more filler (max to 1.0 wt %) was blended.[24] Another report by Sutton et al. proposed a method to modify lignin into photoreactive fillers (i.e., methacrylic anhydride-modified lignin), which could be photopolymerized with a methacrylate resin in the printing process.[25] The reported mechanical tests indicated that the elastic modulus decreased from 0.65 to 0.37 GPa, while the elongation increased from 1.87 to 7.62% with the addition of 15 wt % modified lignin of the printed composites. All of the abovementioned reports had clearly highlighted that on the one hand, lignin plays a crucial role as a sustainable filler in impacting the performance of 3D-printed products. On the other hand, the reinforcing effect of lignin seems complicated depending on the lignin source, content, polymer resin, and the printing techniques used. Moreover, to the best of our knowledge, limited studies[15] have been reported on the effect of incorporation of lignin into stereolithography 3D printing.

In this study, a softwood kraft lignin is applied as a filler in stereolithography 3D printing to reinforce the mechanical properties of printed products. The methacrylate resin was selected for its commercial availability and widespread application in the 3D printing field. Printed samples with slurry blends of lignin and methacrylate resin were prepared, and it was determined that low charges of lignin (0.2−1.0 wt %) could significantly improve the mechanical performance (both Young's modulus and tensile strength) of the fabricated lignin-reinforced composite, which may extend the application of lignin-reinforced stereolithography products. The changes in the fracture morphology of the composites were suggestive of the mechanism of improved mechanical behavior of lignin composite in the 3D printing of these photoreactive resins.

2. RESULTS AND DISCUSSION

2.1. Printability of the Mixed Resin. The blended resin was used to print a "Tennessee" pattern to show the printability of the blended resin. Figure 1a shows that the whole pattern was composed of printed parts with various lignin concentrations (i.e., 0.0, 0.2, 0.5, 0.8, 1.0 wt %). A higher concentration of lignin darkens the printed sample (Figure 1a) and makes the printed sample softer (Figure 1b,c).

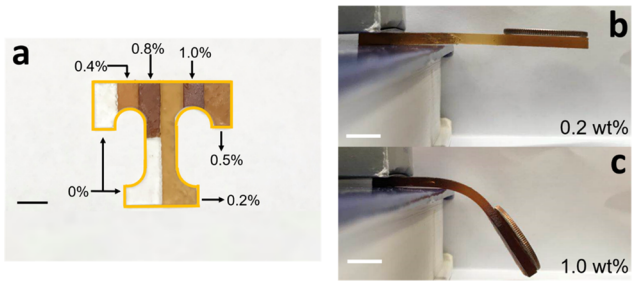

Figure 1. (a) Printed composite with various concentrations of lignin; (b, c) Stiffness estimation of the printed sample with various lignin concentrations by holding the same weight (b-0.2 wt %, c-1.0 wt %). The sample with higher lignin concentration has lower stiffness. All of the scale bars are 1 cm.

2.2. Determination of Lignin Concentration in the Printed Sample. To measure the lignin concentration in the 3D-printed composites, the concentrations of lignin in the printed samples were measured and calculated with the samples N-0.2%, N-0.4%, N-0.5%, N-0.8%, and N-1.0% using UV−vis spectroscopic analysis.[26] The measured results in Table 1 indicated that the lignin concentration in the printed samples is in accordance with the feed ratio, but the measured lignin concentrations were higher than that from the feed ratio. This may be attributed to the settling of lignin in the resin tank by gravity hence lignin was incorporated into the composites during the photopolymerization.

Table 1. Comparison of Feed Ratio in the Printing Resin and Measured Lignin Concentration in Printed Composites

	feed lignin concentration	measured lignin concentration
N-1.0%	1.0 wt %	1.49 ± 0.89 wt %
N-0.8%	0.8 wt %	1.02 ± 0.08 wt %
N-0.5%	0.5 wt %	0.83 ± 0.04 wt %
N-0.4%	0.4 wt %	0.67 ± 0.12 wt %
N-0.2%	0.2 wt %	0.29 ± 0.04 wt %

2.3. Gel Contents and Relative Residual Resin Contents in the Printed Samples. The printed samples consisted of gel fraction that cannot be dissolved (usually cross-linked network) and nongel fraction that can be extracted out using acetone. The gel contents from the printed samples decreased as more lignin was added into the composites (Figure 2). There is ∼98 wt % gel in the printed sample without lignin, which implied that the printed sample by pure resin was highly cross-linked.[27]

With increasing lignin concentration in the composites, less gel was obtained in the printed composites, which indicated that the added lignin likely hindered the cross-linking of the methacrylate resin during the printing, in part, due to the UV absorption of the lignin.[17] This decreased degree of cross-link

DOI: 10.1021/acsomega.9b02455
ACS Omega 2019, 4, 20197−20204

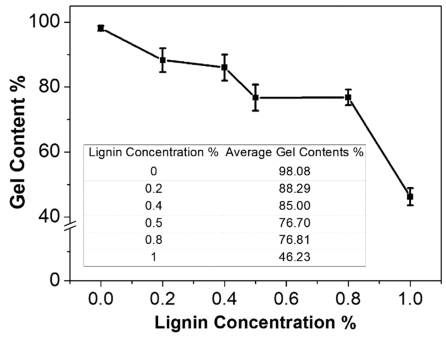

Figure 2. Gel contents of the printed samples with various lignin concentrations.

is consistent with the lower stiffness of the printed samples with higher lignin concentration (Figure 1b).

We then used differential scanning calorimeter (DSC) to investigate the thermal behaviors of printed samples with an attempt to characterize the polymerization status of the nongel part (Figure 3). It has been reported that the unreacted resin in

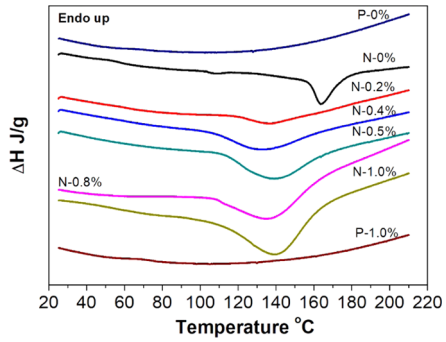

Figure 3. DSC heating curves of several samples.

the printed sample will polymerize when the temperature increases, releasing heat in the processing.[28] As shown in Table 2, all of the non-post-cured samples have exothermic enthalpy,

Table 2. Exothermic Enthalpy and Peak Temperature Collected from the DSC Measurements

sample name	ΔH (J/g)	peak temperature (°C)
N-0%	−14.88	163.5
N-0.2%	−21.58	137.2
N-0.4%	−52.76	133.2
N-0.5%	−66.89	139.2
N-0.8%	−92.64	137.0
N-1.0%	−104.60	140.4

suggesting the presence of unreacted resin in the printed samples. The increased concentration of lignin leads to higher exotherm enthalpy values, which implied that increased amounts of unreacted resin was present in the composites. To confirm this is related to the unreacted resin residual, we ran two postcured printed samples, P-0% and P-1.0%, as well. By contrast, the postcured printed samples have no exothermic behaviors (Figure 3), which can be explained by the relatively low amount of residual resin after UV postcure. In addition, we found that the printed control sample owns an exothermic peak at a higher temperature (163.5 °C), while the other printed samples blended with lignin have exothermic peaks appearing at a lower temperature (137.2−140.4 °C). This phenomenon can be attributed to the low diffusion by the highly cross-linked structure in the control sample, making polymerization in highly cross-linked structures to require more energy (at a higher temperature). Adding lignin in the printed sample caused more residual resin and less-confined (cross-linked) structure, which requires lower energy (thus lower temperature to initiate[28]) for curing the resin.

2.4. FTIR Analysis of the Non-Postcured Samples. Fourier transform infrared spectroscopy (FTIR) analysis was performed for the non-postcured samples, as well as the starting softwood kraft lignin (Figure 4). With regard to the

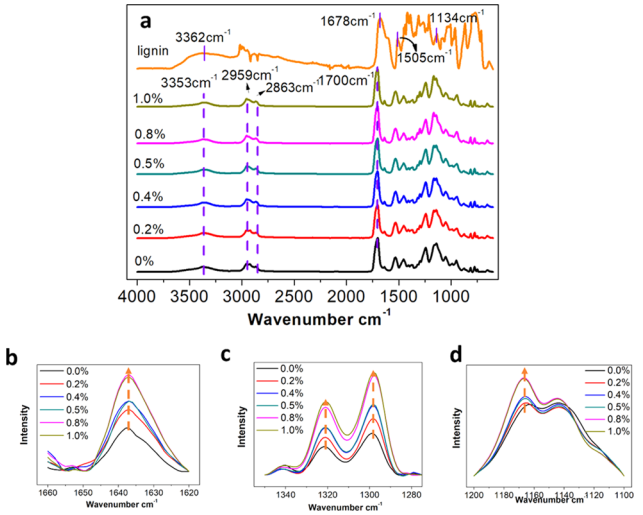

Figure 4. FTIR spectra of printed samples with various concentrations of softwood kraft lignin ((a) 4000−600 cm^{-1}, (b) 1660−1620 cm^{-1}, (c) 1350−1275 cm^{-1}, and (d) 1200−1100 cm^{-1}).

softwood kraft lignin, the hydroxyl, carbonyl, and typical aromatic skeletal vibrations[29] of the kraft lignin were observed at 3362, 1678, and 1505 cm^{-1}, respectively. The aromatic C−H in-plane deformation in the guaiacyl ring at 1134 cm^{-1} of the lignin can also be observed. In the printed samples, the C−H and CH_3 on the backbone of the photoreacted polymer chain were observed at 2959 and 2863 cm^{-1}, respectively. The peaks appearing at 3356 and 1700 cm^{-1} can be attributed to the −OH stretching and C═O stretching, respectively. The −OH stretching was attributed to the adsorption of water and −OH from lignin during the fabrication process, as previously reported.[3,25,28] Due to the low contents of lignin, all of the abovementioned peaks of the printed control sample did not show significant changes of intensities in the spectra compared with the composites incorporated with a different amount of lignin from 0.2 to 1.0 wt %. However, a subtle difference between the printed control sample and the composites was found with respect to the peaks located at 1638 and 1400−1100 cm^{-1}. The minor peak at 1638 cm^{-1} (Figure 4b) represents the stretching of C═C of the residual methacrylate that was not photopolymerized during the printing process,[28] which increased with the increasing amount of lignin added to the printing resin. This was attributed to the presence of lignin that could hinder the photopolymerization process, and the increasing lignin particles interfered with the UV light absorption in the system more significantly. The higher lignin incorporated accompanied by more unreacted residual resin in a printed sample leads to a lower stiffness (Figure 1b,c). With

DOI: 10.1021/acsomega.9b02455
ACS Omega 2019, 4, 20197−20204

respect to the spectra between 1400 and 1100 cm^{-1}, the intensities of the multipeaks at 1350−1275 cm^{-1} (Figure 4c) were assigned to the methacrylate ester and at the side chain of the polymer, which showed a gradual rise as lignin concentration increased. The peak intensity at 1200−1120 cm^{-1} corresponding to the aromatic C−H in-plane deformation of lignin increased with more lignin added (Figure 4d).[25,28] These structural changes in printed samples indicated that the addition of lignin had interfered with the polymerization of methacrylate resin.

2.5. Effects of Lignin on the Tensile Properties of Printed Samples. After the samples were printed, UV postcuring was performed to fully complete the polymerization in the resin, thereby enhancing their mechanical properties.[28] Based on the results (Figure S1), 4 h was chosen for the postcure.

The effects of lignin on the tensile performance of printed samples were analyzed by varying the lignin loading concentration from 0.0 to 1.0 wt % in the resin system and were compared in Figure 5. Comparing the non-postcured and

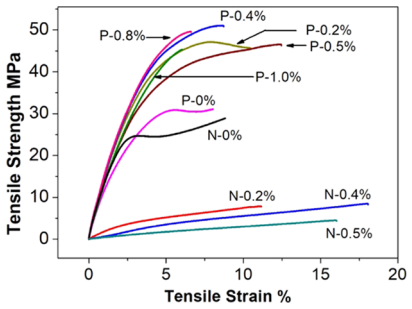

Figure 5. Stress−strain curves for non-postcured and postcured printed samples with various lignin concentrations.

postcured samples, all non-postcured samples exhibit lower tensile strength at the same tensile strain than that of the postcured with the same lignin concentration, and all non-postcured samples show gradually weaker tensile performance as more lignin was added. By contrast, all of the postcured lignin-added samples have a significantly increased ultimate tensile strength at break (45−50 MPa) than the control sample without lignin addition (30.7 MPa). This result indicated that the softwood kraft lignin showed a reinforcing effect to the methacrylate resin in the overall SLA 3D postcured printed samples. Also, the stress−strain curves of P-0% and the P-0.2% show typical yielding before the ultimate break, whereas the other samples with higher lignin addition do not show yielding. This result meant, on one hand, the addition of lignin increased the brittleness of the printed sample, and, on the other hand, there was a lignin concentration threshold beyond which the deformation behavior of the postcured printed sample has been changed.

To further analyze the tensile test results, the tensile strengths and Young's modulus of postcured printed samples are compared in Figure 6 (the data for tensile strength and modulus are recorded in Table 3). With respect to the tensile strength represented in Figure 6a, the tensile strength value of the printed sample without lignin increased from 12.4 to 30.7 MPa after postcuring compared between N-0% and P-0%. This data suggested that the photopolymerization during printing was only partially completed and postcure was necessary to enhance the mechanical properties. Concerning the printed

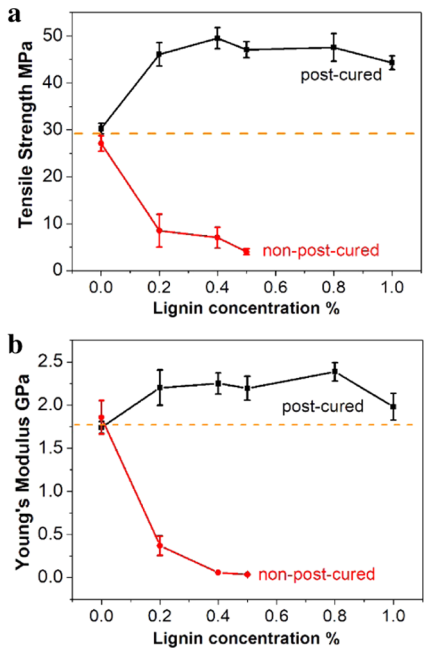

Figure 6. Tensile strength (a) and Young's modulus (b) of non-postcured and postcured printed samples.

composites, the tensile strength showed a gradual decrease as more lignin was added for non-postcured composites. The tendency can be attributed to the hindering effect of the lignin on UV photopolymerization of the resin during printing, which was consistent with the finding in DSC that more residual methacrylate unreacted as more lignin was added. The weaker tensile strength also results in printed samples with more than 0.5 wt % lignin, which cannot be measured on the given load cell for the tensile stress was lower than the minimum stress value can be tested (5 MPa). It showed a similar trend on Young's modulus of the non-postcured samples (Figure 6b).

On the other hand, for postcured printed samples, the tensile strength increased significantly to 46.1 and 49.6 MPa at the lignin incorporation levels of 0.2 and 0.4 wt %, respectively, which are 52 and 64% increment improvement from 30.7 MPa. The tensile strength leveled off by adding more lignin to 1.0 wt %. The incorporation of lignin has also resulted in a remarkable increase of Young's modulus of the printed/postcured samples (Figure 6b). With the addition of 0.2 wt % lignin, Young's modulus increased by 26% from 1.74 to 2.20 GPa. Further increasing the lignin concentration to 0.8 wt % in the resin did not increase the modulus that remained in the range of 2.10−2.50 GPa. However, when 1.0 wt % lignin was added, the modulus steeply decreases to 1.98 GPa. The abovementioned results of the tensile strength and modulus indicated that the incorporation of a small amount of lignin to the methacrylate resin could significantly reinforce the mechanical strength of the postcured printed composites.

2.6. Morphological Analysis of the Fracture Feature of the Printed Samples. To examine the enhancement mechanism of lignin on the printed samples, fractographic analysis of interfacial bonding has been performed using scanning electron microscopy (SEM). P-0.2% was selected to make a comparison with P-0% control as it has shown significant improvement of tensile strength with the lowest lignin concentration. The surface of P-0.2% (Figure 7a) shows observable layer stack gaps every ∼100 μm, which is in

DOI: 10.1021/acsomega.9b02455
ACS Omega 2019, 4, 20197−20204

Table 3. Mechanical Data Collected from Tensile Tests

	tensile strength (MPa)				Young's Modulus (GPa)			
	non-post-cured	increment compared to control (%)	postcured	increasement compared to control (%)	non-post-cured	increment compared to control (%)	postcured	increment compared to control (%)
0	27.1		30.3		1.86		1.74	
0.2	8.5	−68.6	46.1	52.1	0.37	−80.1	2.20	26.4
0.4	7.0	−74.2	49.6	63.7	0.06	−96.8	2.25	29.3
0.5	4.0	−85.2	47.1	55.4	0.04	−97.8	2.19	25.9
0.8	-[a]	-	47.6	57.1			2.39	37.4
1.0	-	-	44.3	46.2			1.98	13.8

[a]- implied strength lower than the minimum stress value can be tested.

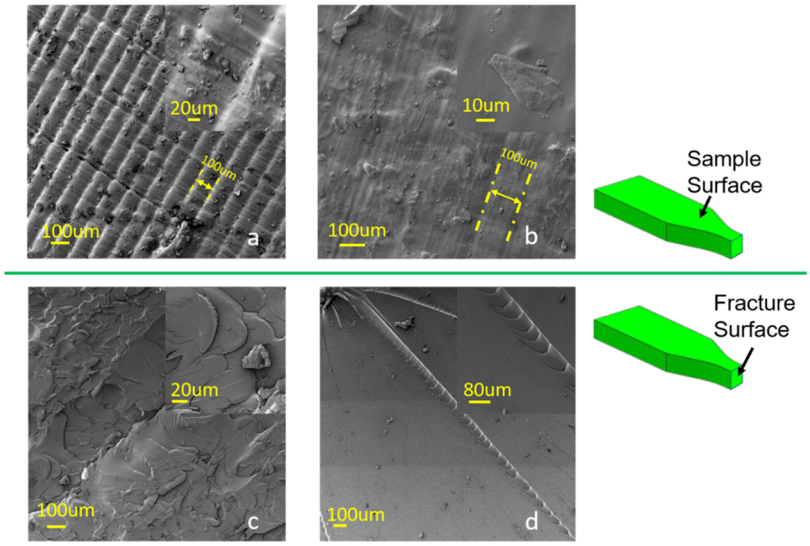

Figure 7. SEM images of the surface (a, b) and cross section (fracture surface) (c, d) of P-0.2% (a, c) and P-0% (b, d).

accordance with the layer thickness (0.1 mm) in printing while layer gaps can only be recognized at some spots in the view as marked in Figure 7b for P-0%. By comparing the sample surface of P-0.2% and P-0%, the surface of P-0.2% was much rougher than that of the control sample. These differences were likely due to the hindering effect of lignin on the UV photopolymerization printing process so that the resin was not fully polymerized. Concerning the fracture surface shown in Figure 7c,d, the fracture surface of both P-0.2% and P-0% showed a typical "brittle" fraction. However, there is some difference between them mainly on crack formation. The control shows a much smoother surface with several long cracks (Figure 7d), while there was some uneven area instead of conspicuous cracks on the failure surface of P-0.2% (Figure 7c). These morphological difference of fracture surfaces can explain, in part, the increase of the tensile strength by the theory of rigid filler particles toughing.[30]

The micromechanism of rigid filler particles toughing includes three steps as stress concentration, debonding, and shear yielding. In this work, adding lignin can affect the stress concentration step during tensile tests. Without lignin addition, the methacrylate resin polymerized into a brittle polymer matrix after postcuring, which resulted in an internal integrity structure that is prone to failure at some weak points with stress loaded. The stress induced on the cross section of the test sample will be concentrated on a few weak points first and then break from there, leaving a smooth surface with a few individual cracks observed in Figure 7d. By contrast, with rigid fillers (i.e., lignin microparticles in this study), the fillers increase the number of stress concentration spots. Then, the stress will be dissipated on more dispersed spots with a more distributed load that prevents the stress concentration microscopically. The well-dispersed lignin fillers at low concentration, therefore, enable the sample bearing higher tensile stress macroscopically. This is possibly the reason that the corresponding fracture surface of P-0.2% was uneven compared with that of the P-0% control. In addition, Manapat et al. found a similar fractographic morphology with printed graphene oxide composite that is related to crack deflection.[9] They concluded that the rough bonding and interactions in the printed sample lead to different stress distribution, which needs more energy for crack propagation, thereby bearing more stress in a tensile test. It seems that the incorporated lignin and graphene oxide played a similar role in dissipating stress load in the composites that are showing enhanced tensile properties.

3. CONCLUSIONS

In this paper, lignin-added methacrylate resin composite with enhanced tensile properties has been fabricated using 3D stereolithography apparatus. The lignin concentration in the composite determined by the UV−vis spectroscopic analysis revealed that the softwood kraft lignin in the range of 0.2−1.0 wt % had been successfully incorporated into methacrylate resin composite. Gel content measurement and DSC tests illustrated that the printed sample without lignin was highly cross-linked with low residual resin but increasing lignin concentration will hinder the cross-link, thus leading to higher residual resin in the printed sample. Postcuring has played a

DOI: 10.1021/acsomega.9b02455
ACS Omega 2019, 4, 20197−20204

considerable influence in completing the photoreaction showing significantly enhanced mechanical properties compared with non-postcured analogs. The addition of lignin had the enhancement of tensile stress of the composite, and the fractographic analysis revealed a rough fracture surface in the lignin-added composite. The added filler at a certain amount is favorable for dissipating stress concentration that could be the primary reason for the enhanced mechanical performance of the lignin-included 3D-printed composites.

4. MATERIALS AND METHODS

4.1. Materials and Chemicals. Softwood kraft lignin was acquired from an industrial source in the southeastern USA and was used after purification following a published methodology.[31] That is, shortly, the received dry kraft lignin was first suspended and stirred in the NaOH solution with EDTA-2Na$^+$. The stirred mixture was then filtrated through a filter paper (Whatman 1), and the filtrate was then gradually acidified to pH = 3.0 with 2 M H_2SO_4 and then stored at −20 °C overnight. After thawing, the precipitates were collected by centrifugation and washed thoroughly with deionized water. The obtained air-dried powder was then used in the following 3D printing procedure. The hydroxyl content on the softwood kraft lignin was characterized by ^{31}P NMR in the Supporting Information (Figure S2 and Table S1).

Photoreactive methacrylate resins (product code: RS-F2-GPCL-04), including methacrylate monomer and oligomer and initiator, were purchased from Formlabs, Inc. Acetone (≥99.5%) and dimethyl sulfoxide (DMSO, ≥99.9%) were supplied by Sigma-Aldrich Inc. 2-Chloro-4,4,5,5-tetramethyl-1,3,2 dioxaphospholane, endo-*N*-hydroxy-5-norbornene-2,3-dicarboximide, pyridine, and deuterated chloroform and chromium acetylacetonate for NMR were all of analytical grade and purchased from Sigma-Aldrich. Isopropyl alcohol (≥99.5%) was provided by Fisher Chemical. All chemicals were used as received.

4.2. Fabrication of Lignin-Dispersed Resins. Lignin was dispersed into the methacrylate resin using a solution-blending procedure. Lignin was first dispersed in acetone at a concentration of 1.00 g/200.00 mL (lignin/acetone), and the resin was dissolved in acetone separately in a ratio of 200.00 g/200.00 mL (resin/acetone). The two solutions were blended independently and stirred overnight at room temperature. The two solutions were then mixed by varying feed ratios to control the lignin concentrations in the resin at 0.0, 0.2, 0.4, 0.5, 0.8, and 1.0 wt %. The resulting mixtures were stirred further overnight followed by rotary evaporation for 4 h at 30 °C to remove the acetone. All of these mixing steps were accomplished in aluminum-foil-covered beakers and flasks to avoid any prepolymerization. To measure the size of lignin in the acetone, dynamic light scattering (DLS) and SEM were used, and the data is shown in the Supporting Information (Figures S3 and S4).

4.3. 3D Printing of the Samples. A stereolithography file (.stl) of the required specimen shape (Type V dogbone in this case) was created in a Siemens NX 10.0 program before 3D printing. The printing processing was controlled by the printer software (Preform, v.2.15.0, Formlabs, Inc.) using a stereolithography printer (Form 1 +, Formlab Inc.) equipped with a 405 nm UV light laser (Figure S5). The 3D printing process included a layer-by-layer UV-light-induced free-radical polymerization of methacrylate resin to form the shape of samples as designed, where the layer thickness, which represents the resolution in the *z*-axis, was chosen as 0.1 mm (Figure S5). After printing, the samples were removed from the platform manually. They were then soaked at room temperature for 10 min in an isopropyl alcohol bath and another 10 min in a second isopropyl alcohol bath to remove unreacted resin on the surfaces of samples following the reported procedure.[25] The obtained sample was then stored in self-made aluminum foil boxes in an ambient environment after air drying overnight and designated as the non-postcured sample.

To postcure the printed samples, a 36 W UV reactor (MelodySusie Co.) equipped with two 9 W lamps centered at a wavelength of 365 nm lamp combined with two 9 W LED centered at a wavelength of 405 nm was used. The UV intensity of the postcure device was measured as 280 ± 16 μW/cm^2 (SP-82UV, Lutron Pocket UV Intensity Meter) during the postcure, and the data is shown in Table S2. The samples were horizontally placed in the light reactor for a certain amount of time to cure one side of the sample, and then the samples are turned over for another period of the same time to cure the other side of the sample. The total postcuring time was presented as the sum up of the two time periods. The non-postcured and postcured samples were designated as N-*x* and P-*x*, respectively, where *x* represented the weight percentage of lignin in the sample corresponding to 0.0, 0.2, 0.4, 0.5, 0.8, and 1.0 wt %. All of the non-post-cured and postcured samples were kept in self-made aluminum foil boxes for further testing.

4.4. Characterization of Printed Samples. *4.4.1. Determination of the Lignin Concentrations in the Printed Sample.* To determine lignin concentration in the printed sample, the uncured printed sample was used because of its higher solubility than the UV cured products in DMSO. The non-postcured samples were first cut into small cubes (approximately 1 mm × 1 mm × 1 mm) and then dissolved into DMSO. The cubes with different lignin blending ratios (N-0.2%, N-0.4%, N-0.5%, N-0.8%, and N-1.0%) were weighed (m_1, ∼0.3 g) and then dissolved in 20.00 mL DMSO with magnetic stirring at room temperature for 24 h. The undissolved material was separated by centrifugation at 10 000 rpm. The supernatant was pipetted out to measure the UV absorption of lignin in the solvent using UV−vis spectrometer at a wavelength of 300 nm with appropriate dilution.[26] The dissolved lignin concentration in the supernatant (q, mg/mL) was determined according to the calibration curve function from softwood kraft lignin/DMSO solution in various concentrations (0.0160, 0.0252, 0.0260, 0.0330, and 0.0365 mg/mL) as described in the Supporting Information (Figure S6). The weight (m_2, g) of the undissolved residue was quantified after vacuum drying at 45 °C until the weights were unchanged. The lignin concentration (c, %) in the printed samples was given by eq 1 with the assumption that the lignin concentration (wt %) in the dissolved products is the same as that left in the undissolved residue

$$c = \frac{q \times V}{(m_1 - m_2) \times 1000} \times 100\% \quad (1)$$

where V is the volume of the solution of the supernatant (20 mL).

4.4.2. Gel Contents. The gel contents of the non-postcured and postcured printed samples were gravimetrically determined after Soxhlet extraction using acetone for 48 h.[27] The

DOI: 10.1021/acsomega.9b02455
ACS Omega 2019, 4, 20197−20204

samples (~0.2 g) were cut into similar size (around 1 mm × 1 mm × 1 mm). The gel contents were calculated using eq 2

$$\text{gel fraction(wt \%)} = (M_1/M_0) \times 100\% \quad (2)$$

in which the M_0 represented the initial weights before the extraction and the M_1 represented the weights after the extraction. The measurement was conducted in triplicates.

4.4.3. Relative Contents of Unreacted Resin in Printing. The relative contents of unreacted resin in the printed sample were evaluated by differential scanning calorimeter (DSC, Diamond, Perkin Elmer), which was calibrated with indium under a nitrogen atmosphere before the tests. The printed samples (3−5 mg) were heated from 25 to 210 °C at 10 °C /min to record the heat flow curves. The polymerization enthalpy was given by the peak area of the exothermic peak during each scan.[28]

4.4.4. Fourier Transform Infrared Spectroscopy (FTIR) Analysis. FTIR analysis of the 3D-printed non-postcured composites was performed on a Perkin Elmer FTIR-ATR spectrometer II at room temperature. The FTIR spectra were collected from 4000 to 600 cm^{-1} with 16 scans and a resolution of 4 cm^{-1}.

4.4.5. Tensile Tests. Tensile testing of the printed samples was performed using a universal testing machine (Instron Co., model: Instron 5567) equipped with a 30 kN load cell according to the ASTM standard D638 (Type V).[32] Dogbone specimens were tested at an ambient temperature using a crosshead speed of 1 mm/min for all of the samples. Young's modulus was obtained by linear fitting of the stress−strain curves in the linear portion of the strain range[33] (0.1−0.5%) in the current study. Young's modulus and tensile strength were determined and reported as an average value of three test specimens.

4.4.6. Scanning Electron Microscopy (SEM). The morphology of the sample and fracture surfaces of the 3D-printed composites were studied using an SEM (Zeiss dual-beam FIB/SEM instrument), with an accelerating voltage of 3 kV. All samples were sputter-coated with a thin layer of gold on the target surface to prevent the buildup of electronic charge before observation.

■ ASSOCIATED CONTENT

Supporting Information

The Supporting Information is available free of charge on the ACS Publications website at DOI: 10.1021/acsomega.9b02455.

^{31}P NMR characterization of the kraft softwood lignin; UV intensity of the postcure UV device; procedure to determine the standard curve of UV absorption−lignin concentration for lignin/DMSO solution; influence of postcuring time in Young's modulus of printed samples with 0.2 wt % lignin (PDF)

■ AUTHOR INFORMATION

Corresponding Author

*E-mail: aragausk@utk.edu.

ORCID

Mi Li: 0000-0001-7523-1266

Arthur J. Ragauskas: 0000-0002-3536-554X

Notes

The authors declare no competing financial interest.

■ ACKNOWLEDGMENTS

The authors thank Prof. Michael Kilbey and Mr. William Ledford at the Department of Chemistry, University of Tennessee, Knoxville, for the help on the DLS measurement.

■ REFERENCES

(1) Ligon, S. C.; Liska, R.; Stampfl, J.; Gurr, M.; Mülhaupt, R. Polymers for 3D Printing and Customized Additive Manufacturing. *Chem. Rev.* **2017**, *117*, 10212−10290.

(2) Wang, X.; Jiang, M.; Zhou, Z.; Gou, J.; Hui, D. 3D printing of polymer matrix composites: A review and prospective. *Composites, Part B* **2017**, *110*, 442−458.

(3) Palaganas, N. B.; Mangadlao, J. D.; de Leon, A. C. C.; Palaganas, J. O.; Pangilinan, K. D.; Lee, Y. J.; Advincula, R. C. 3D Printing of Photocurable Cellulose Nanocrystal Composite for Fabrication of Complex Architectures via Stereolithography. *ACS. Appl. Mater. Interfaces* **2017**, *9*, 34314−34324.

(4) Lin, D.; Jin, S.; Zhang, F.; Wang, C.; Wang, Y.; Zhou, C.; Cheng, G. J. 3D Stereolithography Printing of Graphene Oxide Reinforced Complex Architectures. *Nanotechnology* **2015**, *26*, No. 434003.

(5) Zhang, Y.; Houmin, L.; Xi, Y.; Tao, Z.; Kaiqiang, Z.; Wei, S.; Zhenliang, L.; Houjun, S. Additive manufacturing of carbon nanotube-photopolymer composite radar absorbing materials. *Polym. Compos.* **2018**, *39*, E671−E676.

(6) Choong, Y. Y. C.; Maleksaeedi, S.; Eng, H.; Wei, J.; Su, P.-C. 4D printing of high performance shape memory polymer using stereolithography. *Mater. Des.* **2017**, *126*, 219−225.

(7) Gurr, M.; Hofmann, D.; Ehm, M.; Thomann, Y.; Kübler, R.; Mülhaupt, R. Acrylic nanocomposite resins for use in stereolithography and structural light modulation based rapid prototyping and rapid manufacturing technologies. *Adv. Funct. Mater.* **2008**, *18*, 2390−2397.

(8) Vora, R.; Ashcroft, I.; Hague, R. Investigation of stereolithography material by depth sensing indentation and differential scanning calorimetry. *Plast., Rubber Compos.* **2007**, *36*, 68−76.

(9) Manapat, J. Z.; Mangadlao, J. D.; Tiu, B. D. B.; Tritchler, G. C.; Advincula, R. C. High-Strength Stereolithographic 3D Printed Nanocomposites: Graphene Oxide Metastability. *ACS. Appl. Mater. Interfaces* **2017**, *9*, 10085−10093.

(10) Sandoval, J. H.; Soto, K. F.; Murr, L. E.; Wicker, R. B. Nanotailoring photocrosslinkable epoxy resins with multi-walled carbon nanotubes for stereolithography layered manufacturing. *J. Mater. Sci.* **2007**, *42*, 156−165.

(11) Eng, H.; Maleksaeedi, S.; Yu, S.; Choong, Y. Y. C.; Wiria, F. E.; Tan, C. L. C.; Su, P. C.; Wei, J. 3D Stereolithography of Polymer Composites Reinforced with Orientated Nanoclay. *Procedia Eng.* **2017**, *216*, 1−7.

(12) Yunus, D. E.; Shi, W.; Sohrabi, S.; Liu, Y. Shear induced alignment of short nanofibers in 3D printed polymer composites. *Nanotechnology* **2016**, *27*, No. 495302.

(13) Wang, L.; Ni, X. The effect of the inorganic nanomaterials on the UV-absorption, rheological and mechanical properties of the rapid prototyping epoxy-based composites. *Polym. Bull.* **2017**, *74*, 2063−2079.

(14) Ragauskas, A. J.; Beckham, G. T.; Biddy, M. J.; Chandra, R.; Chen, F.; Davis, M. F.; Davison, B. H.; Dixon, R. A.; Gilna, P.; Keller, M.; et al. Lignin valorization: improving lignin processing in the biorefinery. *Science* **2014**, *344*, No. 1246843.

(15) Yu, P.; He, H.; Jia, Y.; Tian, S.; Chen, J.; Jia, D.; Luo, Y. A comprehensive study on lignin as a green alternative of silica in natural rubber composites. *Polym. Test.* **2016**, *54*, 176−185.

(16) De Chirico, A.; Armanini, M.; Chini, P.; Cioccolo, G.; Provasoli, F.; Audisio, G. Flame retardants for polypropylene based on lignin. *Polym. Degrad. Stab.* **2003**, *79*, 139−145.

(17) Falkehag, S. I.; Marton, J.; Adler, E. Chromophores in Kraft lignin. In *Lignin Structure and Reactions*; American Chemical Society: Atlantic City, 1966; pp 75−89.

DOI: 10.1021/acsomega.9b02455
ACS Omega 2019, 4, 20197−20204

(18) Domínguez-Robles, J.; Martin, N. K.; Fong, M. L.; Stewart, S. A.; Irwin, N. J.; Rial-Hermida, M. I.; Donnelly, R. F.; Larrañeta, E. Antioxidant PLA Composites Containing Lignin for 3D Printing Applications: A Potential Material for Healthcare Applications. *Pharmaceutics* **2019**, *11*, 165.
(19) Xu, W.; Wang, X.; Sandler, N.; Willför, S.; Xu, C. Three-Dimensional Printing of Wood-Derived Biopolymers: A Review Focused on Biomedical Applications. *ACS Sustainable Chem. Eng.* **2018**, *6*, 5663−5680.
(20) Nguyen, N. A.; Barnes, S. H.; Bowland, C. C.; Meek, K. M.; Littrell, K. C.; Keum, J. K.; Naskar, A. K. A path for lignin valorization via additive manufacturing of high-performance sustainable composites with enhanced 3D printability. *Sci. Adv.* **2018**, *4*, No. eaat4967.
(21) Sallem-Idrissi, N.; Sclavons, M.; Debecker, D. P.; Devaux, J. Miscible raw lignin/nylon 6 blends: Thermal and mechanical performances. *J. Appl. Polym. Sci.* **2016**, *133*, No. 42963.
(22) Gkartzou, E.; Koumoulos, E. P.; Charitidis, C. A. Production and 3D printing processing of bio-based thermoplastic filament. *Manufacturing Rev.* **2017**, *4*, 1.
(23) Mimini, V.; Sykacek, E.; Syed Hashim, S. N. A.; Holzweber, J.; Hettegger, H.; Fackler, K.; Potthast, A.; Mundigler, N.; Rosenau, T. Compatibility of Kraft Lignin, Organosolv Lignin and Lignosulfonate With PLA in 3D Printing. *J. Wood Chem. Technol.* **2019**, *39*, 14−30.
(24) Feng, X.; Yang, Z.; Chmely, S.; Wang, Q.; Wang, S.; Xie, Y. Lignin-coated cellulose nanocrystal filled methacrylate composites prepared via 3D stereolithography printing: Mechanical reinforcement and thermal stabilization. *Carbohydr. Polym.* **2017**, *169*, 272−281.
(25) Sutton, J. T.; Rajan, K.; Harper, D. P.; Chmely, S. C. Lignin-Containing Photoactive Resins for 3D Printing by Stereolithography. *ACS. Appl. Mater. Interfaces* **2018**, *10*, 36456−36463.
(26) Sluiter, A.; Hames, B.; Ruiz, R.; Scarlata, C.; Sluiter, J.; Templeton, D.; Crocker, D. *NREL/TP-510-42618 Analytical Procedure − Determination of Structural Carbohydrates and Lignin in Biomass*; NREL: Lakewood, CO, 2012.
(27) Elomaa, L.; Teixeira, S.; Hakala, R.; Korhonen, H.; Grijpma, D. W.; Seppälä, J. V. Preparation of poly(ε-caprolactone)-based tissue engineering scaffolds by stereolithography. *Acta Biomater.* **2011**, *7*, 3850.
(28) Yang, Z.; Wu, G.; Wang, S.; Xu, M.; Feng, X. Dynamic postpolymerization of 3D-printed photopolymer nanocomposites: Effect of cellulose nanocrystal and postcure temperature. *J. Polym. Sci., Part B: Polym. Phys.* **2018**, *56*, 935−946.
(29) Kubo, S.; Kadla, J. F. Hydrogen bonding in lignin: a Fourier transform infrared model compound study. *Biomacromolecules* **2005**, *6*, 2815−2821.
(30) Kim, G. M.; Michler, G. H. Micromechanical deformation processes in toughened and particle-filled semicrystalline polymers: Part 1. Characterization of deformation processes in dependence on phase morphology. *Polymer* **1998**, *39*, 5689−5697.
(31) Wang, Y.-Y.; Li, M.; Cai, C.; Wyman, C.; Ragauskas, A. J. Fast Fractionation of Technical Lignins by Organic Co-solvents. *ACS Sustainable Chem. Eng.* **2018**, *6*, 6064−6072.
(32) ASTM International. *D638 Standard Test Method for Tensile Properties of Plastics*; ASTM International: West Conshohocken, PA, 2014.
(33) Cousins, W. J. Young's modulus of hemicellulose as related to moisture content. *Wood Sci. Technol.* **1978**, *12*, 161−167.

DOI: 10.1021/acsomega.9b02455
ACS Omega 2019, 4, 20197−20204